Unmixing of human skin optical reflectance maps by Non-negative Matrix Factorization algorithm

July Galeano, Romuald Jolivot, Franck Marzani, Yannick Benezeth

Unmixing of Human Skin Optical Reflectance Maps by Non-negative Matrix Factorization Algorithm

July Galeano[a], Romuald Jolivot[b], Franck Marzani[a], Yannick Benezeth[a]

[a]*Le2i, UMR CNRS 6306, Université de Bourgogne, BP 47870, 21078 Dijon Cedex, France*
[b]*National Electronics and Computer Technology Center, 112 Phahonyothin Rd., Pathumthani 12120, Thailand*

Abstract

We present in this paper the decomposition of human skin absorption spectra with a Non-negative Matrix Factorization method. In doing so, we are able to quantify the relative proportion of the main chromophores present in the epidermis and the dermis. We present experimental results showing that we obtain a good estimate of melanin and hemoglobin concentrations. Our approach has been validated by analyzing the human skin absorption spectra in areas of healthy skin and areas affected by melasma on eight patients.

Keywords: Non-negative Matrix Factorization, Spectral Reconstruction, Chromophores quantification, Skin optical reflectance maps.

1. Introduction

Optical reflectance properties of skin can provide valuable information regarding its biochemical composition. This information can be very useful for skin characterization and can contribute to the early detection of a wide-range of pathologies. Interest in the optical reflectance of skin analysis mainly stems from the fact that useful information about skin composition (e.g. melanin, hemoglobin etc.) and physiologic parameters (e.g. color, erythema and pigmentation, etc.) can be obtained in a real-time and non-invasive manner. Applications of the analysis of spectral properties of skin are numerous. For example, measurement of the melanin content in skin is essential in the study of hyper or hypo-pigmentation as well as in the assessment of skin appearance. Melanin is also involved in several human skin pathologies such as malignant melanoma, albinism, vitiligo and melasma. Another important application is the quantitative assessment of inflammation, erythema and occlusion, by means of hemoglobin content and oxygen saturation evaluation. Finally, knowledge of the scattering properties can reveal information about the morphology and architecture of skin, such as arrangement and density of the collagen fibers in the dermis.

The phenomena of light absorption and scattering in human skin can be modeled by the Radiative Transfer Equation (RTE). An inverse analysis of this RTE yields then to the retrieval of tissue optical parameters such as absorption and scattering coefficients. This inverse problem

Email addresses: `july.galeano-zea@u-bourgogne.fr` (July Galeano), `romuald.jolivot@nectec.or.th` (Romuald Jolivot), `franck.marzani@u-bourgogne.fr` (Franck Marzani), `yannick.benezeth@u-bourgogne.fr` (Yannick Benezeth)

can be solved with indirect methods such as Monte Carlo, Kubelka-Munk theory or diffuse theory (Tuchin (2007); Jacques (2009); Wang et al. (1995); Jacques and Pogue (2008)). Also, simplest methods based on the Beer-Lambert law have been used for light-skin interaction analysis. As example, linear regression and statistical approaches have been used for the analysis of changes in the concentration of melanin and hemoglobin in reflectance spectra (Shimada et al. (2000); Tsumura et al. (1999)).

Human skin can be represented as a scattered multilayered structure. Consequently, it is possible to study the interaction between light and the chromophores (pigments) composing these layers. Several chromophores absorb light in skin. However, the main chromophores affecting the reflectance spectra in the visible light wavelength range are melanin and hemoglobin (Zonios and Dimou (2009)).

We propose in this paper the use of a Blind Source Separation (BSS) algorithm for the quantification of the main chromophores in epidermis and dermis. We especially study in this paper the use of a Non-negative Matrix Factorization (NMF) algorithm. Then, we present experimental results showing that the obtained concentration maps are a good estimate of melanin and hemoglobin concentration.

The reflectance maps have been acquired using a Hyper-Spectral Imaging (HSI) system named ASCLEPIOS (Analysis of Skin Characteristics by Light Emission and Processing of Images Of Spectrum) (Jolivot et al. (2011b)). This system consists of two parts. First, Multi-Spectral Images (MSI) are acquired by an optical setup composed of a light source, a filter wheel, and a monochromatic camera. Then, a Hyper-Spectral Cube (HSC) is generated by a neural network-based algorithm.

Melanin, which is a pigment present in the epidermis and responsible for the assessment of skin color, have shown its strong relation with melasma. Melasma is a tan or dark skin discoloration and occurs as a result of excess melanin production in skin cells. Consequently, we experimentally validate the chromophores quantification with NMF by analyzing the amount of melanin in areas of healthy skin and areas affected by melasma. The human skin data used in this analysis have been obtained from 8 volunteers affected with melasma lesions on their cheeks.

The paper is organized as follows. We present in section 2 the Hyper-Spectral data acquisition system and its experimental validation. Then, in section 3, we present the decomposition of human skin reflectance maps in proportion of the main chromophores present in epidermis and dermis by using NMF algorithm. Finally, section 4 presents experimental results showing that the obtained concentration maps are a good estimate of melanin and hemoglobin concentration. It is also presented an analysis of these chromophore concentrations in areas of healthy skin and areas affected by melasma from eight volunteers.

2. Hyper-Spectral Data Acquisition System

2.1. Principle

Visible reflectance maps from human skin have been acquired by a Hyper-Spectral Imaging (HSI) system named ASCLEPIOS (Jolivot et al. (2011b)). The acquisition system is illustrated in Fig. 1. It consists of two parts: the acquisition of Multi-Spectral Images (MSI) by an optical setup, and the generation of a Hyper-Spectral Cube (HSC) by a neural network-based algorithm.

The optical setup for the MSI acquisition system is composed of a light source, a filter wheel, and a monochromatic camera. Light source corresponds to a xenon arc lamp with light spectrum in the range of 380 to 800 nm. This light is filtered consecutively by 10 interference filters placed in the revolving wheel. The Full Width at Half Maximum of each filter is 80 nm.

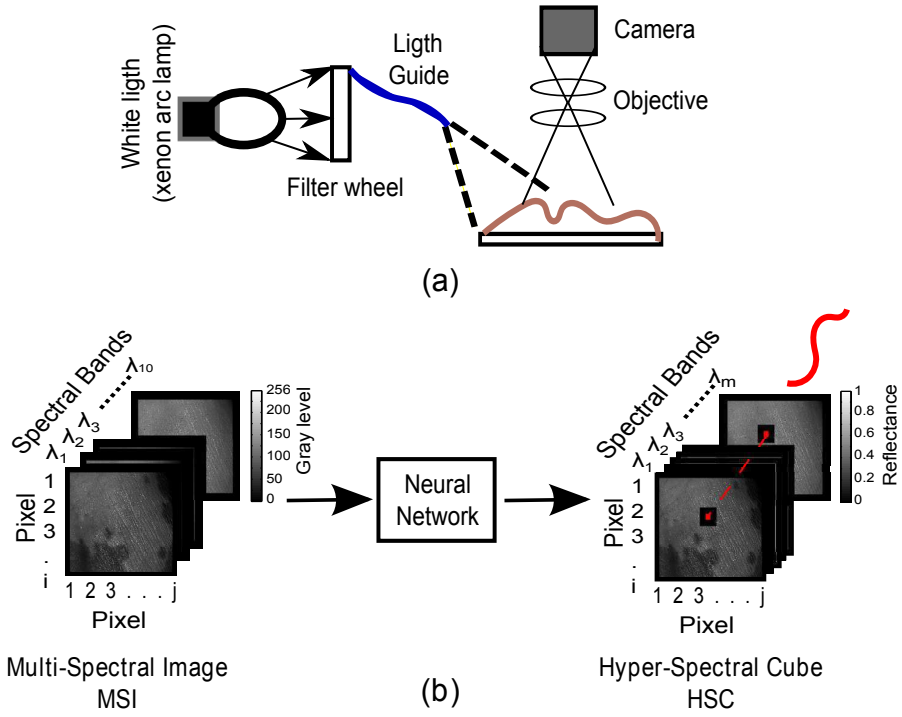

Figure 1: ASCLEPIOS system configuration. (a) Optical set-up for the acquisition of Multi-Spectral Images from human skin sample. (b) Generation of a Hyper-Spectral Cube by a neural network-based algorithm (Mansouri et al. (2005)). The HSC gives the visible reflectance map at each wavelength.

The filtered light is transported through a light guide illuminating the object of interest. Then, monoband images of a Region Of Interest (ROI) are acquired using a monochromatic camera with an ad-hoc optical objective with built-in chromatic correction over the entire operating wavelength range.The system has been previously calibrated at each filter. In this way, the systematic noise affecting the reconstruction of the reflectance spectrum at each pixel is removed. Non uniform illumination of the system are also calibrated. The ROI size is $38 \times 32 mm^2$. This set of 10 monoband images constitutes the MSI. The acquisition of a MSI lasts less than 2 seconds. Therefore, if the patient is properly installed, we can consider that the scene is completely static.

These MSI are then processed by a neural network-based algorithm (Mansouri et al. (2005)) which aims is to retrieve, from the camera signal, the reflectance spectrum at each pixel of the ROI. In this way, the HSC (i, j, λ) is formed, where i and j denote the spatial dimensions and λ the spectral one. In doing so, we obtain at each bandwidth the spatial map of reflectance values from the evaluated ROI.

The neural network is composed of two steps: learning and reconstruction. The learning process involves the use of a set of $P = 24$ patches (GretagMacBeth ColorChecker®) which represent various spectra whose spectral properties are known. From this set of patches, two acquisitions are performed. A first one by a spectrophotometer providing N values of spectral reflectance curve for each patch (p_i). This first acquisition yields to a learning matrix R $(N \times P)$. The second acquisiton corresponds to 24 MSI (a MSI for each patch p_i), each one containing

K ($K = 10$) gray level values obtained from the averaged HSC at each patch. The later leads to a matrix D ($K \times P$). These matrices constitute then a set of corresponding pair (input D and expected-output R data) used by the neural network to perform a supervised learning. The learning stops when it reaches the minimum of the validation error. Once learned, neural network outputs a coefficient matrix Q (called synaptic coefficient matrix) of size $[N \times K]$.

The reconstruction of an Hyper-Spectral Cube is fast and simple because the operation is a product between the coefficient matrix and the camera response or Multi-Spectral input values. The implemented reconstruction function is flexible and allows different sampling rate from 10 to 1 nm yielding reconstructed spectra of N values (ranging from 36 to 400 respectively).

Within the framework of this work, the estimated HSC is composed of 36 bands between 430 and 780 nm. The Full Width at Half Maximum of each band is 10 nm. The spatial resolution of the HSC is 1312×1082 pixels.

2.2. System validation

The spectral accuracy of the reconstructed HSC has been evaluated on 150 healthy volunteers (Jolivot et al. (2011a)). The participants have been classified based on their Skin PhotoTypes (SPT) following the Fitzpatrick Scale (Fitzpatrick (1975)). The population covers from SPT II (lightly pigmented) to SPT VI (highly pigmented). Table 1 presents the SPT distribution of the 150 volunteers. The validation of the system is performed by comparing data acquired using a commercial spectrophotometer (CM 2600d, Minolta) and the average HSC issued from ASCLEPIOS system. The use of healthy skin areas guarantee homogeneity in the Hyper-Spectral Cube. The acquisition is performed at three different body locations: two skin areas exposed to the sun (hand, face) and one area non exposed to the sun (lower back).

Table 1: SPT distribution of the 150 volunteers.

SPT Type	II	III	IV	V	VI
Nb	18	21	56	41	14

The quality of the reconstructed HSC is evaluated with the Goodness of Fit Coefficient (GFC). The metric uses the commercial spectrophotometer data as reference. The GFC is based on the Schwartz's inequality and is defined by the following formula:

$$GFC = \frac{\left|\sum_j R_m(\lambda_j) R_r(\lambda_j)\right|}{\left(\sum_j \left[R_m(\lambda_j)\right]^2\right)^{1/2} \left(\sum_j \left[R_r(\lambda_j)\right]^2\right)^{1/2}} \quad (1)$$

where $R_m(\lambda_j)$ is the spectrum value measured with the spectrophotometer at wavelength λ_j and $R_r(\lambda_j)$ is the reconstructed spectra value, by the neural network, at wavelength λ_j. This criterion is bounded between 0 and 1, and consequently provides an easy interpretation.

We present, in Table 2, the GFC values for each SPT. According to Hernandez et al. (Hernández-Andrés et al. (2001)), reconstruction with GFC higher than 0.99 is considered good. Consequently, this study validates the accuracy of ASCLEPIOS system to reconstruct Hyper-Spectral Cubes of cutaneous data. Such cubes provide both spatial and spectral information which can be used to retrieve skin component maps.

Table 2: GFC for each location and each SPT and average of all SPT.

	GFC Values		
SPT	Hand	Face	Back
I	0.9977	0.9963	0.9963
II	0.9977	0.9963	0.9963
III	0.9980	0.9972	0.9974
IV	0.9976	0.9972	0.9975
V	0.9971	0.9971	0.9980
VI	0.9972	0.9977	0.9975
Average	0.9975	0.9971	0.9975

3. Reflectance map unmixing

Human skin is described as a scattering multi-layered media composed of different pigments. The main pigments affecting the visible spectrum are melanin and hemoglobin (Zonios and Dimou (2009)). These two pigments are present in the first two layers of skin: epidermis and dermis respectively (Martelli et al. (2010); Shimada et al. (2001)).

When light interacts with skin, light travels through the different layers where scattering, absorption, and reflection occur. Since ASCLEPIOS sytem acquires reflectance $R(\lambda)$ spectrum as the ratio of reflected to incident energy, absorbance spectrum $A(\lambda)$ can be estimated from reflectance by equation 2 (Anderson et al. (1981)):

$$A(\lambda) = -10 \log(R(\lambda)). \tag{2}$$

This absorbance spectrum $A(\lambda)$ can be stated as the sum of absorbance of each layer (Shimada et al. (2001); Tuchin (2007)) based on the modified Beer-Lambert law:

$$A(\lambda) = \sum_{i=1}^{n} C_i A_i(\lambda) + G \tag{3}$$

where $A_i(\lambda)$ is related to the molar absorption coefficient of pigments present at layer i, together with its scattering effect (Tuchin (2007)). C_i accounts for the concentration of the absorber, and G represents the remaining components (i.e. water, bilirubine, etc) not individually defined in the model. n is the number of layers.

Based on this fundamental linear model, we apply Non-negative Matrix Factorization (NMF) in order to retrieve the contributions to the spectral absorption given by epidermis and dermis. As far as we know, NMF have not been used for the decomposition of the human skin absorbance spectrum but have been widely used, for example, in the analysis of geological components (Keshava and Mustard (2002); Pauca et al. (2006); Yang et al. (2011)) or more recently on biological tissues analysis for autofluorescence removal (Montcuquet et al. (2011)). Actually, this method is particularly well suited to our problem because it relies on the non-negativity of the data, which is a constraint validated by the physical meaning of absorbance spectra.

The main goal of Blind Source Separation (BSS) methods is to represent a given signal as a weighted sum of main sources. If we decompose into two sources, we can say from Eq. 3

that these sources correspond to the main chromophores in the epidermis and dermis. From a mathematical point of view, BSS approximates a given $n \times m$ matrix Y, with $Y_{nm} \geq 0$, into the product of two non-negative matrices $W \in R^{n \times r}$ (matrix of weighted coefficients W_{nr}) and $H \in R^{r \times m}$ (matrix of main sources H_{rm}), i.e. $Y \approx WH$ (Lee and Seung (1999); Lin (2007); Wang and Zou (2008)).

NMF finds the matrices W and H by minimizing the difference between Y and WH:

$$f(W, H) \equiv \frac{1}{2} \|Y - WH\|_F^2 \tag{4}$$

where $\|\cdot\|_F$ is the Frobenius norm.

In a simple way, the minimum of the cost function $f(W, H)$ can be found by updating the terms W and H with the following gradient descent step:

$$\begin{aligned} W &\longleftarrow W - \beta_W \tfrac{\delta f(W,H)}{\delta W} \\ H &\longleftarrow H - \beta_H \tfrac{\delta f(W,H)}{\delta H} \end{aligned} \tag{5}$$

with β an update factor given for each element of matrices W and H; the terms $\frac{\delta f(W,H)}{\delta W}$ and $\frac{\delta f(W,H)}{\delta H}$ given by:

$$\begin{aligned} \tfrac{\delta f(W,H)}{\delta w_{nr}} &= -[YH^T - WHH^T]_{nr} \\ \tfrac{\delta f(W,H)}{\delta h_{rm}} &= -[W^T Y - W^T WH]_{rm}. \end{aligned} \tag{6}$$

Alternative to gradient descent step, a multiplicative update rule has been proposed by Lee and Seung (1999) to overcome the sensitivity of the gradient descent step size. The multiplicative update proposes then to choose the factor β for matrices W and H as:

$$\begin{aligned} \beta_{nr} &= \tfrac{w_{nr}}{[WHH^T]_{nr}} \\ \beta_{rm} &= \tfrac{h_{rm}}{[W^T WH]_{rm}}. \end{aligned} \tag{7}$$

With equations (6) and (7) in eqution (5), we obtain the following multiplicative update rule:

$$\begin{aligned} W_{nr} &\leftarrow W_{nr} \tfrac{(YH^T)_{nr}}{(WHH^T)_{nr}} \\ H_{rm} &\leftarrow H_{rm} \tfrac{(W^T Y)_{rm}}{(W^T WH)_{rm}}. \end{aligned} \tag{8}$$

Equation (4) can be modified in several ways depending on the application. As a result, penalties can be added in order to enforce sparseness or smoothness of matrices W and/or H (Pauca et al. (2006)). In our case, we use smoothness penalty in matrix H. The use of this penalty is reflected in the cost function with:

$$f(W, H) = \frac{1}{2} \|Y - WH\|_F^2 + \frac{1}{2} \alpha \sum_{rm} H \tag{9}$$

where setting α to 1 give us the better results in our application.

Solving this modified cost function in equation (9), the multiplicative update presented in equation (8) becomes:

$$W_{nr} \leftarrow W_{nr} \frac{(YH^T)_{nr}}{(WHH^T)_{nr}}$$
$$H_{rm} \leftarrow H_{rm} \frac{(W^T Y)_{rm} - H_{rm}}{(W^T WH)_{rm}} \tag{10}$$

which is the iteration process used in this article.

As depicted in Fig. 2, the $n \times m$ matrix Y is the bidimensional representation of the HSC obtained with ASCLEPIOS system. The number of columns of matrix Y corresponds to the number of spectral bands (36 in this case). Each column of this matrix represents the spatial distribution of absorption values at the given spectral band.

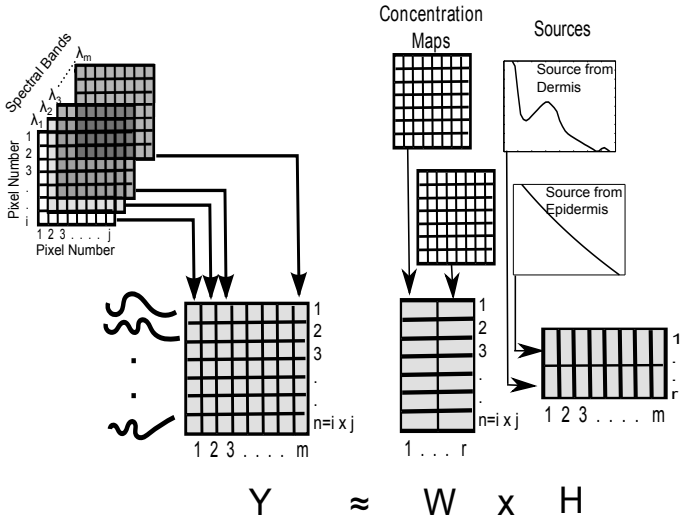

Figure 2: Principle of the decomposition of human skin absorption spectra with a Non-negative Matrix Factorization method. The spectrum obtained for each pixel of a Hyper-Spectral Cube (Y) is observed as the weighted sum of principal components in the epidermis and dermis. NMF algorithm obtains the average spectra of those principal components (H), together with their respective quantification at each pixel of the Hyper-Spectral Cube (concentration maps W).

Each line of matrix H contains the estimated absorption spectra of the main components of epidermis and dermis. We present in section 4 experimental results showing that these two sources are a good estimate of melanin and hemoglobin. Finally, matrix W presents in each column the estimated proportions of these sources at each pixel of the ROI.

In the following, matrix Y is the HSC measured with ASCLEPIOS, and the multiplication $W \times H$ is the estimated HSC.

4. Results and Discussion

Using ASCLEPIOS system, Hyper-Spectral Cubes (HSC) were obtained from 8 patients with skin photoypes between III and V. These data are used as a reference to validate the performance

of NMF. From the measured HSC, ROI of (but not limited to) 90×90 *pixels* (8100 spectra) were analyzed using the iterative relation presented in equation 10. The spectrum associated with each pixel of the HSC is considered as a linear combination of the main pigments present in the epidemis and the dermis. For each measured HSC, we obtain the average spectra of these main components (matrix H in equation 10) and their relative concentration maps (matrix W in equation 10).

We first present in section 4.1 a spectral analysis of the main sources in order to prove that the absorption spectra that we obtain are a good estimation of hemoglobin and melanin. Next, we present in section 4.2 an analysis of the concentration maps calculated over areas of healthy skin and areas of skin affected by melasma.

4.1. Spectral analysis

Using two layers in the linear model presented in equation 3, we retrieve the contributions to the spectral absorption given by epidermis and dermis. The main pigments affecting the visible spectrum are hemoglobin in the dermis and melanin in the epidermis (Martelli et al. (2010); Shimada et al. (2001)). We first present the absorbance spectra obtained with NMF on one patient in Fig. 3. These absorbance spectra have been calculated over three different ROI: healthy/melasma, melasma and healthy.

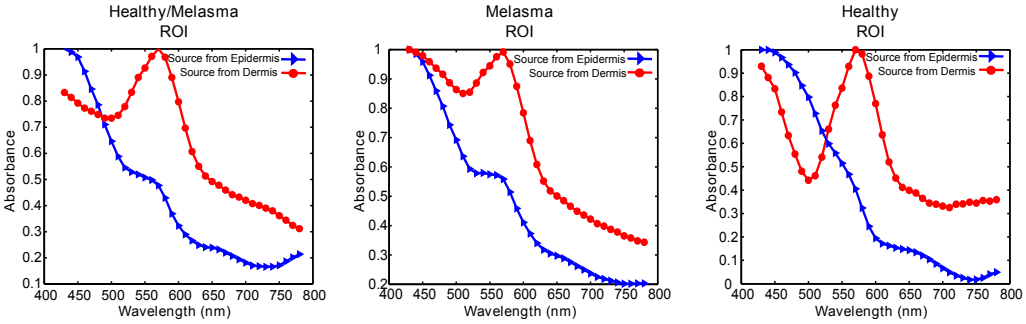

Figure 3: Absorbance spectra obtained with NMF.

It is possible to observe that absorbance spectra presented in Fig. 3 are a good approximation of melanin (blue line with triangles) and hemoglobin (red line with circles). The estimated melanin absorption spectrum presents a decay of 50% around 550 nm and the estimated hemoglobin absorption spectrum presents a characteristic peak around 450 and 570 nm. These observations are consistent with their theoretical absorption spectra.

Quantitative comparison between the theoretical absorption spectra of hemoglobin and melanin and the calculated spectra obtained on all patients is presented in Table 3 and 4. Table 3 presents quantitative results obtained on areas of healthy skin while Table 4 presents results obtained on areas of skin affected by melasma. Three correlation coefficients are calculated as follows: a first one corresponds to the degree of correlation between the calculated ($W \times H$ in equation (10)) and the measured HSC (Y in equation (10)); second and third ones are calculated between the theoretical and estimated melanin-hemoglobin absorbance spectra. Correlation coefficients are calcultated with:

$$r = \left(\frac{\sum_{i=1}^{N} (Re_i - \overline{Re})(Rt_i - \overline{Rt})}{\sqrt{\sum_{i=1}^{N} ((Re_i - \overline{Re})^2)} \sqrt{\sum_{i=1}^{N} ((Rt_i - \overline{Rt})^2)}} \right)^2 \tag{11}$$

where Re is the estimated data and Rt is the theoretical one. $\overline{Re}$ and $\overline{Rt}$ are the mean value of the estimated and theorical data respectively. This coefficient is bounded between 0 and 1, with 1 its best value.

Table 3: Degree of correlation between: the calculated-measured human skin absorption spectra, and the theoretical-estimated melanin-hemoglobin absorbance spectra obtained on healthy skin areas.

	Healthy Area Correlation Result		
Patient Number	Mean absorption Spectra	Melanin	Hemoglobin
1	0.99	0.93	0.91
2	0.99	0.94	0.94
3	0.99	0.88	0.91
4	0.99	0.97	0.94
5	0.99	0.96	0.92
6	0.99	0.98	0.90
7	0.99	0.97	0.94
8	0.99	0.96	0.86

Table 4: Degree of correlation between: the calculated-measured human skin absorption spectra, and the theoretical-estimated melanin-hemoglobin absorbance spectra obtained on areas of skin affected by melasma.

	Melasma Area Correlation Result		
Patient Number	Mean absorption Spectra	Melanin	Hemoglobin
1	0.99	0.95	0.94
2	0.99	0.98	0.94
3	0.99	0.97	0.82
4	0.98	0.97	0.85
5	0.99	0.96	0.90
6	0.99	0.98	0.93
7	0.99	0.86	0.94
8	0.99	0.97	0.90

The correlation coefficients presented in Tables 3 and 4 between the theoretical absorption spectra of melanin and hemoglobin, and the first and second sources of our decomposition, are

higher than 0.9. Consequently, this result validates that the obtained sources are a good estimate of melanin and hemoglobin in case of areas of healthy skin and also on areas of skin affected by melasma. Then, because the correlation coefficients between the reconstructed HSC (given by $W \times H$ in equation (10)) and the measured one (Y in equation (10)) are also higher than 0.9, we can conclude that the NMF converges efficiently, taking into account that they have been started with random values.

4.2. Concentration maps analysis

We present in this section an analysis of the concentration maps obtained by the reflectance maps decomposition on areas of healthy skin and areas of skin affected by melasma. Fig. 4 presents the estimated concentration maps of melanin and hemoglobin on three different ROI of one patient (Patient 8 in Tables 3 and 4): healthy/melasma, melasma, and healthy skin areas.

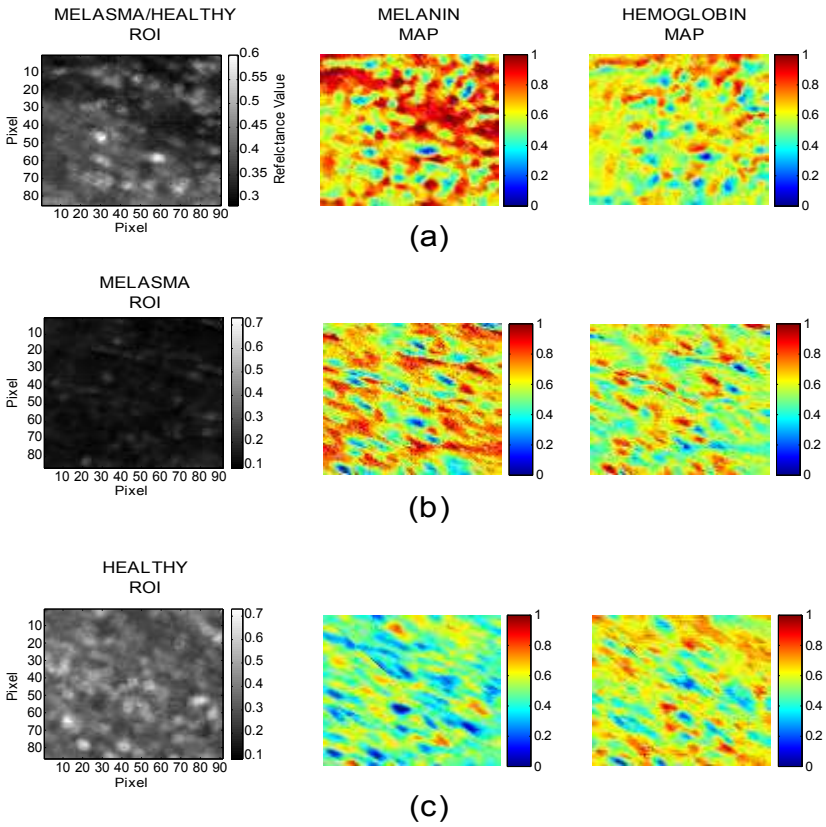

Figure 4: Concentration maps of melanin and hemoglobin in healthy/melasma, melasma and healthy ROI. In the healthy/melasma ROI, the upper-right part of the ROI is affected by melasma. The first column presents the 3 ROI while the second and third ones present respectively the melanin and hemoglobin concentration maps. The scale is normalized between 0 (dark blue) and 1 (dark red).

It is possible to observe that the areas affected by melasma present higher concentration of melanin than healthy areas while the hemoglobin concentration remains the same. This obser-

vation is consistent with the histological cause of melasma: an increased amount of melanin component (Miyachi (2009)). We present in Fig. 5 the concentration map histograms on the healthy and melasma ROI. We can observe that the concentration peak of melanin is higher (approximatively 0.62) in the melasma ROI than in the healthy ROI (approximatively 0.44). There is a increase of almost 41%, i.e, a ratio of melanin of 1.4 between normal skin area and melasma one. This observation is also consistent with the histological cause of melasma: an increase epidermal melanin pigmentation in lesional skin. According to the literature this increase can range between 35% to 81% in skin phototype from II to V (Kang and Ortonne (2010); Miot et al. (2007)).

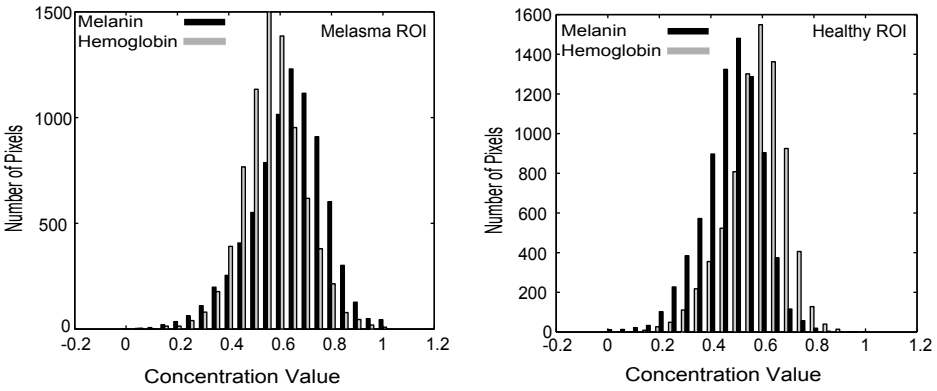

Figure 5: Histograms of melanin and hemoglobin concentration maps in melasma and healthy skin ROI.

Finally, we present in Fig. 6 the concentration values of melanin versus hemoglobin obtained for healthy (blue) and melasma (red) ROI from one patient. Interestingly, these concentration values are a potential indicator about the classification between healthy and melasma area. Nevertheless, it is important to note that the hemoglobin should not be considered for the diagnosis of melasma but, as the concentration values obtained by our method are relative (between the two main sources), it is the ratio between the concentration of melanin and hemoglobin that can be used for classification between a healthy area and an area suffering from melasma.

5. Conclusions and Further Work

Non-negative Matrix Factorization (NMF) is presented as a potential method in the study of human skin optical absorbance maps. Analyses were done on visible absorbance maps from eight patients affected by melasma. Those maps were acquired by a Hyper-Spectral acquisition system called ASCLEPIOS, which capacity in providing both spectral and spatial information is demonstrated.

Using a multiplicative update approach over a ROI, relative quantities of the principal pigments underlying dermis and epidermis are obtained together with their average spectrum. Those spectra together with their respective relative quantities lead to the estimation of absorbance maps of the ROI under study. This fact allowed us to corroborate the performance of NMF by comparing the estimated maps with respect to the ones obtained with ASCLEPIOS system. Results demonstrated a degree of correlation higher than 90% between both maps.

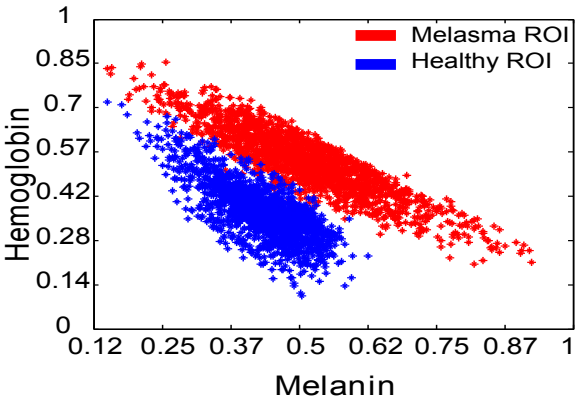

Figure 6: Melanin Vs. Hemoglobin concentration values in melasma and healthy regions of interest in one patient.

Because it is well-known that Melasma is characterized by excess of melanin in the epidermis (Miyachi (2009)), the method was validated analyzing the obtained melanin and hemoglobin concentration maps, over healthy and melasma ROI of the data provided by the eight patients. Experimental results agree with the histological cause of melasma. Consequently, the proposed method could be used on pathologies for which the quantification of melanin is important, especially when this is difficult with the naked eye.
Future works will focus on validation of the estimated pigment concentration using for example skin phantoms and also on monitoring over time of pathologies associated with pigmentation problems.

Acknowledgments

We would like to thank the cooperation given by Dr. R. Baba and Dr. N. Shamsudin from the Department of Dermatology at Kuala Lumpur Hospital. Also we would like to acknowledge the assistance given by Professor Ahmad Fadzil and Hermawan Nugroho from Universiti Teknologi Petronas, and Dr. Norashikin from the faculty of Medicine and Health Sciences at Universiti Putra Malaysia.

The authors would like also to thank the financial support provided by *Conseil Regional de Bourgogne*-France, and *Fond Européen de Développement Regional (FEDER)*-France.

Anderson, R., Hu, J., Parrish, J., 1981. Optical radiation transfer in the human skin and applications in in vivo remittance spectroscopy. In: Bioengineering and the skin: based on the proceedings of the European Society for Dermatological Research symposium. Springer, p. 253.

Fitzpatrick, T., 1975. Soleil et peau. Journal de Medecine Esthetique 2, 33–34.

Hernández-Andrés, J., Romero, J., Raymond L.Lee, J., 2001. Colorimetric and spectroradiometric characteristics of narrow-field-of-view clear skylight in granada, spain. J. Opt. Soc. Am. A 18 (2), 412–420.

Jacques, S., 2009. Spectral imaging and analysis to yield tissue optical properties. Journal of Innovative Optical Health Sciences 2 (2), 123–129.

Jacques, S., Pogue, B., 2008. Tutorial on diffuse light transport. Journal of biomedical optics 13, 041302.

Jolivot, R., Nugroho, H., Vabres, P., Fadzil, M., Marzani, F., 2011a. Validation of a 2d multispectral camera: application to dermatology/cosmetology on a population covering five skin phototypes. In: Proceedings of SPIE. Vol. 8087. p. 808729.

Jolivot, R., Vabres, P., Marzani, F., 2011b. Reconstruction of hyperspectral cutaneous data from an artificial neural network-based multispectral imaging system. Computerized Medical Imaging and Graphics 35 (2), 85–88.

Kang, H., Ortonne, J., 2010. What should be considered in treatment of melasma. Annals of dermatology 22 (4), 373.

Keshava, N., Mustard, J., 2002. Spectral unmixing. Signal Processing Magazine, IEEE 19 (1), 44–57.
Lee, D., Seung, H., 1999. Learning the parts of objects by non-negative matrix factorization. Nature 401 (6755), 788–791.
Lin, C., 2007. Projected gradient methods for nonnegative matrix factorization. Neural Computation 19 (10), 2756–2779.
Mansouri, A., Marzani, F., Gouton, P., 2005. Neural networks in two cascade algorithms for spectral reflectance reconstruction. In: Image Processing, 2005. ICIP 2005. IEEE International Conference on. Vol. 2. pp. II–718.
Martelli, F., Del Bianco, S., Ismaelli, A., Zaccanti, G., 2010. Light Propagation through Biological Tissue and Other Diffusive Media.
Miot, L., Miot, H., Silva, M., Marques, M., 2007. Morphological and functional comparative study of melanocytes in melasma lesions. Anais Brasileiros de Dermatologia 82 (6), 529–534.
Miyachi, Y., 2009. Therapy of Skin Diseases. Springer Verlag.
Montcuquet, A., Herv'e, L., Navarro, F., Dinten, J., Mars, J., 2011. In vivo fluorescence spectra unmixing and autofluorescence removal by sparse nonnegative matrix factorization. IEEE Transactions on Biomedical Engineering 58, 2554–2565.
Pauca, V., Piper, J., Plemmons, R., 2006. Nonnegative matrix factorization for spectral data analysis. Linear Algebra and its Applications 416 (1), 29–47.
Shimada, M., Masuda, Y., Yamada, Y., Itoh, M., Takahashi, M., Yatagai, T., 2000. Explanation of human skin color by multiple linear regression analysis based on the modified Lambert-Beer law. Optical Review 7 (4), 348–352.
Shimada, M., Yamada, Y., Itoh, M., Yatagai, T., 2001. Physics in Medicine and Biology 46, 2385.
Tsumura, N., Haneishi, H., Miyake, Y., 1999. Independent-component analysis of skin color image. JOSA A 16 (9), 2169–2176.
Tuchin, V., 2007. Tissue optics: light scattering methods and instruments for medical diagnosis. SPIE, Bellingham, Washington.
Wang, L., Jacques, S., Zheng, L., 1995. Mcml–monte carlo modeling of light transport in multi-layered tissues. Computer methods and programs in biomedicine 47 (2), 131–146.
Wang, W., Zou, X., 2008. Non-negative matrix factorization based on projected nonlinear conjugate gradient algorithm. In: ICA Research Network International Workshop (ICARN 2008). pp. 5–8.
Yang, Z., Zhou, G., Xie, S., Ding, S., Yang, J.-M., Zhang, J., 2011. Blind spectral unmixing based on sparse nonnegative matrix factorization. IEEE Transactions on Image Processing 20, 1112–1125.
Zonios, G., Dimou, A., 2009. Light scattering spectroscopy of human skin in vivo. Optics Express 17 (3), 1256–1267.